Convective fractionation during magnetite and hematite dissolution in silicate melts

C. H. DONALDSON

School of Geography and Geology, University of St. Andrews, Fife KY16 9ST, Scotland

Abstract

Single crystals of magnetite and of hematite have been dissolved at atmospheric pressure in superheated melts in the systems $CaO–MgO–Al_2O_3–SiO_2$ and $CaO–Al_2O_3–SiO_2$, and in a basalt. The crystals were suspended in alumina crucibles containing *ca* 3.5 cm^3 of melt. Quenched run products were examined optically and by electron probe analysis to establish the distribution of Fe in the glassy charges. There is usually a concentration of Fe at the base of a run product, consistent with flow of dissolved matter from the crystal to the floor. One or more columns of brown, Fe-rich glass may extend from the underside of a relic crystal towards the floor. In CMAS run products, such columns typically extend this entire distance, whereas in the CAS and basalt run products, the columns are either detached from the crystal or do not reach the floor. In the CMAS melt (viscosity ~1 poise) there is apparently continuous release of Fe-bearing melt from around a dissolving crystal, whereas in the CAS and basalt melts (viscosities 7000 and 300 poise, respectively) release is intermittent. In CMAS run products the Fe content is usually greatest, in glass, at the base, and declines gradually upwards; in CAS and basalt runs the bottom of a crucible is occupied by discrete, sharply bounded pillows of Fe-rich glass, with only slight, or no, gradation in composition. Rising gas bubbles can elevate small blobs of the denser, Fe-bearing melt from around a dissolving crystal, and trains of bubbles in the CAS melt may guide this Fe-bearing melt, against gravity, to the surface of the charge. When the bubbles burst at the surface, this dense melt is left in an unstable location and releases diapirs which descend to the bottom of the crucible. In spite of the evidence that convective fractionation occurs in these haplomagmas and in the basalt, it remains to be demonstrated that it will occur during sidewall crystallization or during the growth of minerals in a cumulus mush to cause magmatic differentiation.

KEYWORDS: fractionation, magnetite, hematite, silicate melts, magmatic differentiation.

Introduction

SEVERAL experimental petrologists exploring the dissolution of minerals in silicate melts have shown that, above the liquidus temperature of a melt, dissolution rate [*d*(radius)/*d*(time)] is constant with time (Kuo and Kirkpatrick, 1985*a,b*; Donaldson, 1985, 1986; Brearley and Scarfe, 1986). It has also been found that the solute-enriched compositional boundary layer (or 'film' for short) of melt that forms around a dissolving crystal is essentially of constant thickness, regardless of run duration. As chemical diffusion-limited dissolution rate would result in an ever-thickening film, these observations imply that another process of material transport must operate. The preferred explanation has been that the difference in composition, and hence density, between the film and the melt beyond it causes melt in the film to flow spontaneously from around the crystal.

This mechanism of melt transport has also been invoked by those exploring the fluid dynamics of solidifying magma chambers; that is, a crystal growing in a magma may generate a solute-depleted compositional boundary layer which peels away from the crystal due to the buoyancy contrast with the bulk of the melt (e.g. McBirney and Noyes, 1979; McBirney, 1980; Sparkes *et al.*, 1984). In the materials science literature, this process is well known and has been variously referred to as *solutal convection* (Carruthers, 1976), *thermosolutal convection* (Coriell *et al.*, 1980) and *chemical convection* (Rosenberger, 1979). In the petrological literature, the term *compositional convection* has been introduced (Tait *et al.*, 1984). As a petrological process this flow is important when the migrating boundary

Mineralogical Magazine, September 1993, Vol. 57, pp. 469–488

layer melt remains separate from the bulk melt and collects, along with the melt from many other crystals, as a compositionally discrete volume of magma (McBirney, 1980). The terms *convective fractionation* (Rice, 1981; Sparks *et al.*, 1984) and *liquid fractionation* (McBirney *et al.*, 1985) have been proposed for this mechanism of magmatic differentiation.

Ordinarily a temperature boundary layer will also exist in the melt adjacent to a crystal (Coriell *et al.*, 1980), enhancing or diminishing the buoyancy of the chemical boundary layer. However, as thermal diffusion is much faster than chemical diffusion the width of the thermal boundary layer will be so large that the temperature difference across the chemical boundary layer will be minimal and hence have no effect on the density of melt within it.

Whereas plumes of solute-depleted liquid can sometimes be seen rising from crystals growing in aqueous solutions at room temperature (e.g. McBirney, 1980; Tait *et al.*, 1985; Lawrence and Birnie, 1989; Tait and Jaupart, 1989), this is not so in molten silicate solutions because the progress of an experiment cannot be observed. In the only attempt ever to establish whether compositional convection can occur from around a crystal immersed in silicate melt, Donaldson and Hamilton (1987) conducted experiments in which a rod of silica glass suspended vertically in picrite melt partially dissolved, creating differentiated run products. These consist of a layer of homogeneous, uncontaminated picrite glass, surmounted by a layer of more siliceous glass down through which the silica content declines to the content of the picrite. It was proposed that the differentiation resulted from segregation of silica-enriched buoyant melt in the boundary layer which envelopes the rod. This melt would rise along the rod to the surface of the charge and spread out across the meniscus, forming a steadily thickening horizontal layer.

In those experiments the silica rod penetrated the meniscus rather than being immersed in the picrite, so there were no plumes or patches of silica-enriched glass within the picrite glass to prove that segregation had occurred by buoyancy. Thus an alternative explanation remains feasible, namely that segregation was driven by unequal surface tension on the meniscus arising from fluctuations in the composition of melt on the surface (Jebsen-Marwedl, 1956). Unequal surface tension would cause motion of melt across the meniscus so as to eradicate any compositional differences but this would also generate motion to some depth below the surface (probably up to a few mm; Rosenberger, 1979), which could perpetuate the flow of silica-rich melt from around the dissolving rod. Fluid motion for this reason is referred to as *surface tension convection, or S convection* (Rosenberger, 1979), or *Marangoni convection* (*cf.* Donaldson and Henderson, 1988). In the picrite–silica glass rod experiments, reactions between melt and gas at the meniscus (e.g. reduction of Fe^{3+} to Fe^{2+}) could have caused surface tension variations and hence convection.

This paper reports on new dissolution experiments designed to obtain unequivocal evidence of the operation of 'pure' compositional convection, i.e. unassisted by either thermal convection or S-convection. The results show for the first time that this process does indeed operate in silicate melts, strengthening the view that it can contribute to magmatic differentiation involving crystal–liquid processes.

Experimental procedures and limitations

Materials

Crystals of magnetite (0.2 wt.% TiO_2) or hematite (2.8 wt.% TiO_2, <0.1% Al_2O_3 and <0.1% MnO) were partially dissolved in three kinds of melt, one is in the system CaO–MgO–Al_2O_3–SiO_2 (CMAS), another is in CaO–Al_2O_3–SiO_2 (CAS) and the third is a basalt. Lacking transition metal cations, the first two melts are colourless, whereas magnetite/hematite dissolution releases iron ions that locally tint the melts brown. If chemical diffusion is the only mechanism transporting iron from the crystal–melt interface, then brown glass in a quenched run product will be found only in the film around the crystal, and its colour intensity will decrease away from the crystal. On the other hand, if any coloured melt flowed out of the film around the crystal it would be obvious in a run product. In the basalt melt, release of iron from a magnetite or hematite crystal to melt, darkens the glass sufficiently so that the result of any flow of melt out of the film around a crystal will be detected in thin section.

The artificial melts were prepared as glasses from reagent-grade oxides by repeated grinding and fusion. The basalt, which was used as finely powdered rock, was oxidised in air at 800 °C for 24 hours before use. Analyses of the CMAS and CAS glasses and of fused basalt are contained in Table 1, and Table 2 lists the liquidus temperature of each melt, with computed densities and viscosities at three temperatures. The melts cover a useful range of physical properties. The Fe-free melts differ in density by 10% but whereas the viscosity of the CAS melt is moderate, like that of

andesite or basaltic andesite melt, that of the CMAS melt is extremely low, comparable to the viscosities of komatiite and lunar high-Ti basalt melts. The viscosity and density of the basalt are intermediate to those of the artificial melts.

The conditions of the runs conducted, and generalised synopses of their outcomes are given in Table 3

Method

All experiments were conducted in air, at atmospheric pressure, in a furnace fitted with a pneumatic elevator that eases the hearth smoothly in and out of the furnace. Cylindrical crucibles of alumina, 1.8 cm in diameter and 2.4 cm tall, were used as sample containers. Temperature measurements made with a thermocouple at 1400 °C show that the base of a crucible in contact with the hearth is approximately 3 °C cooler than 1 cm above the hearth and 4 °C cooler than 2 cm above the hearth. The orientation of this temperature gradient precludes thermal convection.

To prevent a dissolving crystal from touching either the melt meniscus, or the floor or the side of the crucible it must be tethered within a crucible (Fig. 1). Crystal cuboids of side 3–4 mm cut from larger crystals were drilled with a 0.8 mm-diameter, diamond-tipped dental drill bit

Table 1: Electron microprobe analyses in wt.% of synthetic and natural glass starting materials prepared by fusion in air and quenching in water.

	A	B	C
SiO_2	40.4	62.1	50.9
TiO_2	-	-	1.9
Al_2O_3	15.4	14.5	15.6
FeO	-	-	10.5
MgO	14.8	-	6.1
CaO	29.2	23.3	9.3
Na_2O	-	-	3.1
K_2O	-	-	1.1
Total	99.8	99.9	98.5

A - CMAS system) Made by repeated fusion and grinding of
) oxide mixes
B - CAS system)

C - Basalt from Cleish Hills, Saline, Fife

Analyses made on Jeol Superprobe with mineral standards. All Fe as Fe^{2+}

Table 2: Liquidus temperature, computed density and computed viscosity of each melt at 1 bar.

		CMAS	CAS	Basalt
$T_{liquidus}$, °C		1300[a]	1170[a]	1270±10[b]
Density[c] gcm^{-3}	1350°C	2.759	2.513	2.581
	1400	2.742	2.502	2.571
	1450	2.725	2.492	2.561
Viscosity[d] poise	1350°C	4.7	5370	125
	1400	3.4	2970	80
	1450	2.5	1700	50

a - taken from phase diagram (Levins *et al.* 1969)
b - from melting experiment with rock powder
c - by method of Bottinga and Weill (1970), using partial molar volumes of Mo *et al.* (1982)
d - by method of Shaw (1972)

Table 3: Summary of runs conducted and their general appearance

Melt	Crystal	Run T range °C	Run t range hr	No. of runs	General appearance of run products
CMAS	Magnetite	1420 - 1470	0.5 - 1.5	4	The glass varies in colour upwards from deep brown at the base through light brown to lemon yellow and in some instances to colourless at the top. When incompletely dissolved, a crystal is surrounded by a narrow layer of deep brown glass of non-uniform thickness (100-500 μm); narrow threads (100-400 μm thick) of brown glass may extend from the underside of the crystal, in some instances to the crucible base.
CMAS	Hematite	1390 - 1450	0.4 - 6.5	9	
CAS	Magnetite	1330	1.8 - 6.5	4	In short runs a froth of air bubbles with colourless and brown glass septa covers the meniscus. In longer runs the meniscus is smooth and streaked with brown glass in the manner of an oil slick; brown glass pendants may hang down or be detached from the meniscus, and have fed a brown layer of glass at the base. If the crystal is incompletely dissolved, a thread of brown glass may extend from the underside part way to the base of the crucible.
CAS	Hematite	1280 - 1400	0.5 - 17	18	
Basalt	Magnetite	1300 - 1350	3 - 8.2	2	The chestnut-brown glass is never visibly zoned, either optically or in BSE image, nonetheless, individual probe analyses reveal a concentration of Fe in the lower reaches of charges. One charge contains a dark pillow of Fe-enriched glass lying on the base of the crucible, with a short tongue of the same glass extending from the underside of the partially dissolved crystal. Slight accumulation of yellow Al_2O_3-enriched melt is visible below the meniscus.
Basalt	Hematite	1280 - 1325	4.5 - 166	4	

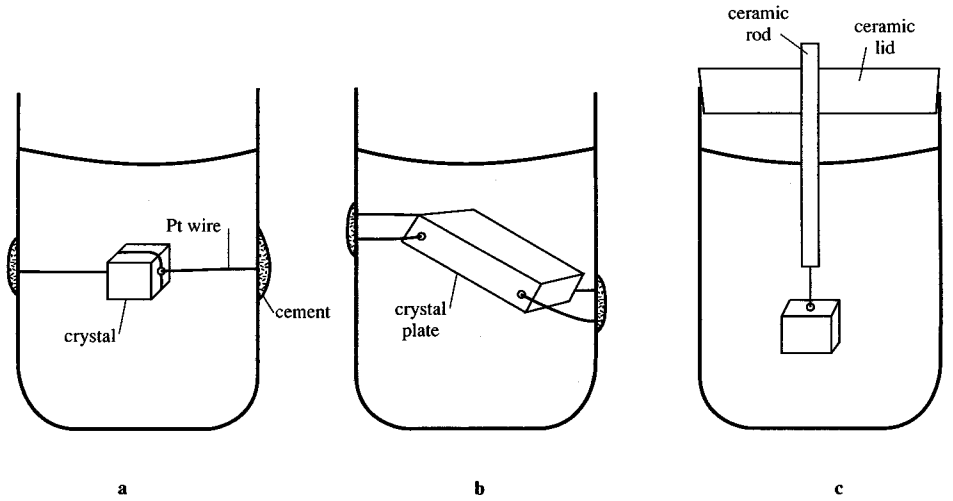

FIG. 1. Three means used to suspend a crystal in a crucible of melt.

and threaded with 0.05 mm PtRh alloy wire. The ends of the wire were passed through holes drilled on either side of the crucible and then tied on the outside of the crucible. The holes were re-sealed with high-temperature alumina cement (Figs. 1*a*,*b*).

Some experiments were conducted with a tabular piece of crystal, with the largest surface either inclined or approximately horizontal. In these, two holes were drilled, one on either end of the crystal and each was threaded with a wire that passed through holes drilled in the crucible wall (Fig. 1*b*).

Two other methods of supporting crystals were tried unsuccessfully. In one, the crystal was wrapped tightly in platinum wire and hung from above the meniscus. This proved unsuccessful when air bubbles that almost invariably adhere to a crystal would drag it to the meniscus, where it would remain throughout an experiment. In another method the wire was passed through a thin ceramic tube (Fig. 1*c*) to prevent the crystal from floating to the meniscus. This too proved unsuitable as air bubbles would buoy up the crystal until it touched the side of the tube, whereupon the Fe-rich melt produced by the dissolution would flow along the tube's surface, and eventually spread out over the meniscus. (Indeed, unless the tube was plugged, some of the Fe-rich melt would flow up the interior of the tube and emerge at its top.)

A crucible, with a crystal tethered in position, is filled with small pieces of glass or powdered basalt and placed in the furnace. Much air is released on melting, so that after several minutes the crucible must be removed from the furnace, topped up with glass, or basalt powder, and returned to the furnace. This action is repeated once more to ensure the crucible is almost filled with melt.

A maximum run duration is imposed by the fact that the cement used to plug holes drilled in the crucible is porous, allowing melt to soak through to the outside of the crucible and eventually flow over its exterior. Depending on temperature, it takes approximately 5–10 hours for CMAS melt to saturate the cement at which time the experiment has to be terminated; the more viscous CAS melt can be run for 4–5 times longer. Throughout an experiment there will be a slow drawdown of melt in the crucible which could interfere with other flows of interest.

A run is quenched by removing the crucible from the furnace into air. A visual estimate of the cooling rate is about 60 °C s^{-1}, based on the time it takes for the glass to stop glowing. To inhibit formation of cracks, the crucible is cooled more slowly from the glass transition temperature to *ca.* 150 °C by placing it on top of the furnace with a larger inverted crucible as a cover. (Attempts to force the cooling rate proved unhelpful and were abandoned: plunging the crucible into water causes shattering of both the crucible and its contents, and cooling in an air jet creates so many fractures in both glass and crucible that the charge is too fragile to handle.)

A crucible is cut in half along a vertical plane using a thin-bladed rotary saw and each half impregnated with glue to seal cracks. Both halves of CMAS and CAS charges are then photographed with powerful illumination shone

through the rear of the crucible; basalt samples are opaque at this stage. Finally a 2 mm-thick slice is cut from one half and prepared as a polished thin section for further documentation using photography, electron microprobe analysis and back-scattered electron (BSE) imaging. BSE imaging of CMAS and basalt charges did not reveal boundary layers and other chemical heterogeneities, but did in some CAS system charges.

For some runs, the approximate crystal dissolution rate has been estimated from the change in its size. The rate ranges from ~100–1000 μm hr^{-1}, depending on temperature and the melt used (CMAS most rapid, CAS least).

None of the melts used is saturated with alumina and so each must dissolve some of the crucible during a run. The existence of an Al-enriched, 200–500 μm-thick film of glass adjacent to the walls confirms this. However, the rate at which dissolution occurs must be extremely slow as there is no measurable decrease in the nominal thickness of the wall following an experiment, and neither is there evidence of flux-line attack where the meniscus intersects the wall. Furthermore, with the exception of the basalt (see later) there is no measurable concentration of Al in glass at the meniscus, even though it would be expected that the Al-enriched melt formed along the wall should ascend due to buoyancy. Thus any compositional convection that has occurred due to crucible dissolution is unlikely to have interfered with any caused by the dissolving magnetite–hematite crystals.

Bubbles

As in most work with silicate melts, bubbles form, move, coalesce, and burst at the melt–air contact. All runs must have experienced some forced convection as a consequence of bubbles ascending. Decomposition of hematite to magnetite, which might happen in runs below 1390 °C (Deer *et al.*, 1964), would release oxygen which could form bubbles rather than dissolving in the melt. However, regardless of run temperature, bubbles are found in all run products, both those with magnetite and those with hematite. Oxygen may also be released from the basalt by reduction of some ferric iron at the higher temperature employed in an experiment compared to that used to oxidise the basalt powder. However, the principal source of the bubbles is air, originally present between the particles of glass or rock powder loaded into a crucible.

In the CMAS and basalt systems most of a run product is essentially bubble-free, indicating that bubbles rose quickly to the surface. The meniscus is typically bubble-free, except in very short runs (e.g. <0.5 hr), implying that bubbles collapse almost instantly at the melt–air interface. Within a charge, however, there may be a few bubbles (0.1–1 mm in diameter), either trapped on the underside of a crystal or adhering to its top or sides.

Bubbles are generally abundant in runs with the more viscous CAS melt, and often the meniscus is covered in a 1–5 mm-thick froth. Bubbles rise more slowly in this melt and evidently are slower to burst at the meniscus. Though there may be several large bubbles adhering to a crystal, those within the charge (0.1–0.2 mm) are generally much smaller than those in the froth (0.5–2 mm), implying that small bubbles coalesce in the froth before bursting at the melt surface.

Rising bubbles could drag boundary layer melt from around a dissolving crystal into the bulk of the melt, creating a false impression of the operation of compositional convection. Thus considerable effort was devoted to attempts to reduce the problem. Some experiments were conducted with initial fusion at up to 100 °C above the intended run temperature for up to 10 min before cooling to the run temperature, so that the reduced viscosity would speed removal of the bubbles. Another approach was to prepare bubble-free starting glass (by long duration melting) and then to core out cylindrical plugs of glass just less than the inner diameter of the alumina crucible. One plug with part of its top hollowed out was placed in the bottom of the crucible; a crystal was then inserted in the hollow and wired into the crucible, and finally a second plug with a hollowed-out base was placed on top of the crystal. While these elaborate procedures helped to reduce the number of bubbles in the CAS run products, they neither eliminated them nor succeeded in preventing the creation of large bubbles adhering to crystals. Consequently, neither procedure was adopted for most runs.

Conclusion

The experimental procedures used are, of necessity, a compromise rather than being ideal. This is because of the need to contain the melt, because of the need to immerse the crystal in the melt and because of the necessary small scale of the technique. The reader is cautioned that although it is tempting to view the run products as models of magma chambers, the scales are quite different. Strictly, the experiments explore only what can happen at the scale of the individual crystal.

One reviewer of the manuscript questioned whether the experimental results could apply to dissolution and melting processes involving magmas in nature, arguing that the substantial superheating employed in the experiments to speed dissolution depolymerizes the melts, converting them from Bingham-body flow characteristics (finite yield strength) to Newtonian characteristics (no yield strength). Kerr and Lister (1991) re-assessed whether magmas at liquidus and subliquidus temperatures genuinely possess a yield strength, as reported by several experimental investigators from laboratory and field measurements. They concluded that magmas do not, except when a touching framework of crystals exists, i.e. after several tens of per cent crystallisation. Thus the influence of superheat in the experiments reported here should not create flow characteristics different from those of magma, either at its liquidus or within a few tens of degrees below its liquidus.

Results

CMAS system

When a crystal dissolves completely, the product glass is coloured, dark brown at the crucible base, grading upwards to yellow or through yellow to colourless. In the black and white photographs used in this account, the differences in contrast imperfectly disclose these colour variations (Fig. 2*a*). The variations accurately record the asymmetric vertical distribution of iron in the glass (e.g. Fig. 3*a*). The most dense, least viscous and most Fe-rich melt was at the base of the crucible (2.780 g cm^{-3}, 1.3 poise) and was overlain by progressively less dense and less Fe-rich melt. In some charges, the Fe concentration declines through the entire thickness of the glass, and in others reaches background level (effectively zero) well below the meniscus. While molten, this was a stable situation with no tendency for overturn and mixing.

Since crystals are not located on the base of a crucible during an experiment, the observed vertical variations in Fe content cannot be ascribed to chemical diffusion during a run. The cause is revealed in run products with a relic crystal (Fig. 2). These, too, grade upwards from brown, Fe-enriched glass to yellow and to colourless glass; however, the basal brown glass is connected by a brown column to a film of brown glass that surrounds the crystal. Such products show that contaminated melt, formed in contact with a crystal as it dissolves, can drain away in a plume that descends to the floor, where it spreads out displacing the colourless melt upwards. Preserved in such run products, is a record of convective fractionation.

It could be argued that plumes originate when a crucible is disturbed during quenching. However, the presence of brown glass on the bottom of a crucible in a run in which the crystal was totally dissolved (Fig. 2*a*) means that plumes do form *during* experiments.

Estimates of the thickness of the film of Fe-enriched glass surrounding a crystal were made by optical examination in a thin section, and range from 50–500 μm. There is difficulty in pinpointing the limit of a film, and comparison of visual estimates with others obtained by chemical traverses through a film suggest that the former have a 25% uncertainty. Generally a film is not uniform in thickness around a crystal. It tends to be thinner on top and along the sides of a crystal than on the bottom. Lobes may extend from the bottom of a crystal or from the overhanging face of an inclined crystal (e.g. Figs. 2 and 3).

Table 4 gives examples of chemical analyses obtained of glass close to a crystal. Regardless of film thickness and of where on the crystal–glass interface an analysis is made, the glass composition is essentially the same, suggesting that crystal–melt surface equilibrium existed. Differences in density and viscosity across films are summarised in Table 5.

Chemical variation has been explored within the brown vertical columns. Analyses along the axis of a column usually differ from one another and may bear no relation to height in the column (e.g. Fig. 3*c*); this is not unexpected as columns are not perfectly vertical, and so a thin section will not include the true axis (i.e. core) of the column everywhere. Generally, the measured iron content of the axis is less than that of glass on the inside of the film surrounding a crystal but it may closely approach that value. Across a column the most Fe-rich glass is always in the axis and to either side the Fe content declines sharply to the background value (Fig. 3*d*). In none of the traverses made is there other than a continuous decline from axis to margin. There is no indication that columns get thicker downwards, as might be expected if entrainment of surrounding melt occurred.

Most run products are not entirely free of bubbles in the glass, although there is never froth on the meniscus. Small, isolated bubbles may exist anywhere in a charge, although large ones tend to be located within the brown film on the underside of a crystal (e.g. Figs. 3*b* and *c*). Some small bubbles are attached to a narrow column of yellow, Fe-bearing glass, dragged from the film of

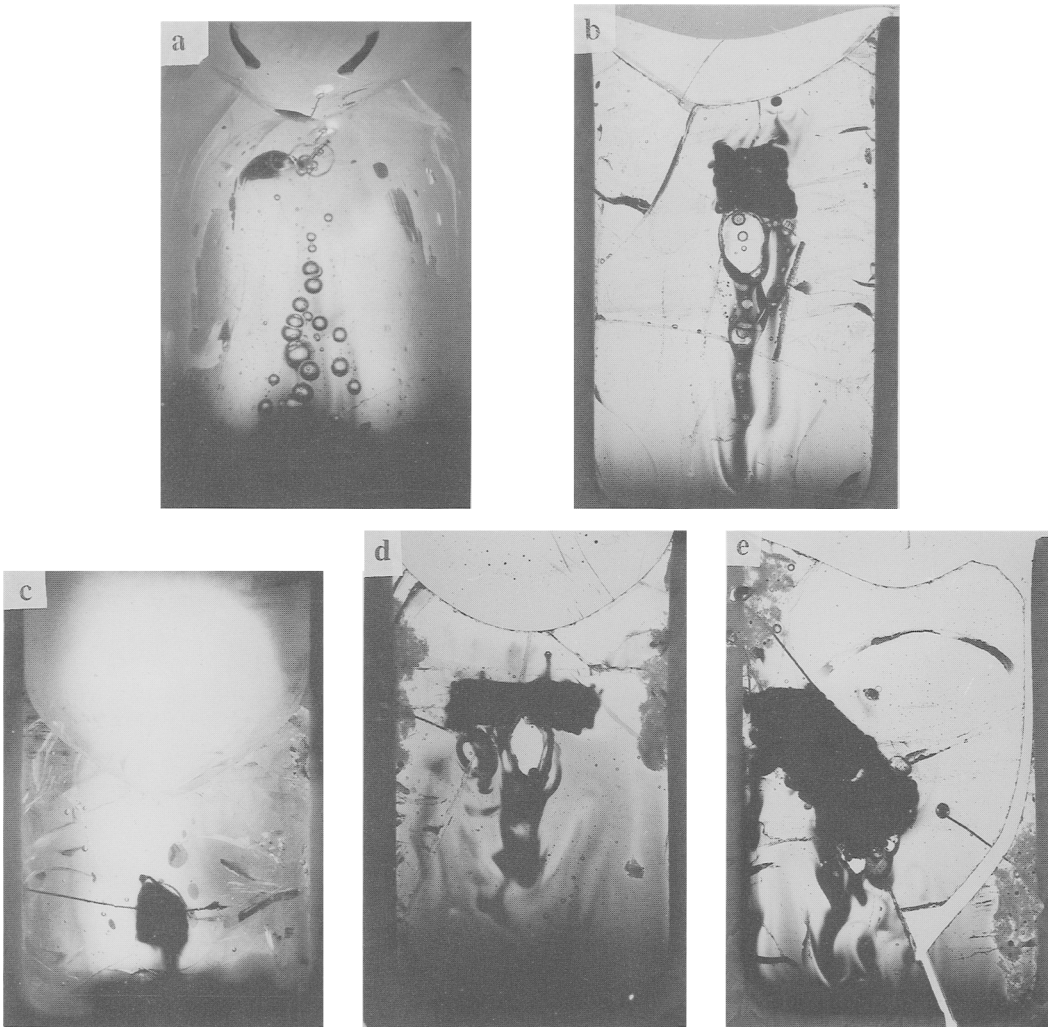

FIG. 2. Selected run products of CMAS experiments: (*a*) magnetite, 1450°, 1.6 hr; (*b*) magnetite, 1430°, 1.3 hr; (*c*) hematite, 1450°, 0.5 hr; (*d*) magnetite, 1450°, 0.5 hr; (*e*) magnetite, 1450°, 0.5 hr. Width of views is 18 mm.

melt around a crystal, or out of the layer of Fe-bearing melt that accumulates at the floor. This example of 'two-phase convection' (Grout, 1918) offers an explanation for the existence in some charges of yellow blobs above a crystal, and of some charges in which the meniscus is streaked with yellow–brown glass, doubtless carried there by bubbles that burst subsequently.

Where a large bubble exists below the brown film on the underside of a crystal, it is frequently part of a column of brown glass (Fig. 3*b*). The upper reaches of the bubble touch the film, its surface is coated with a thin film (<20 μm) of brown glass, and the brown column extends from the bottom of the bubble. During a run, melt from the underside of the crystal must move over the surface of the bubble probably by a combination of flow under gravity and by surface tension convection, and must then escape from the bottom of the bubble. The origin of the bubble–column relationship is unclear: it may be that one or more large bubbles rising beneath a crystal encounter the film around the crystal and initiate column formation by withdrawing melt by S-convection; alternatively, a column may begin when an instability in the film grows into a column, sweeping small bubbles down it which then aggregate, creating enough buoyancy to rise against the flow and form a large bubble on the underside of a crystal.

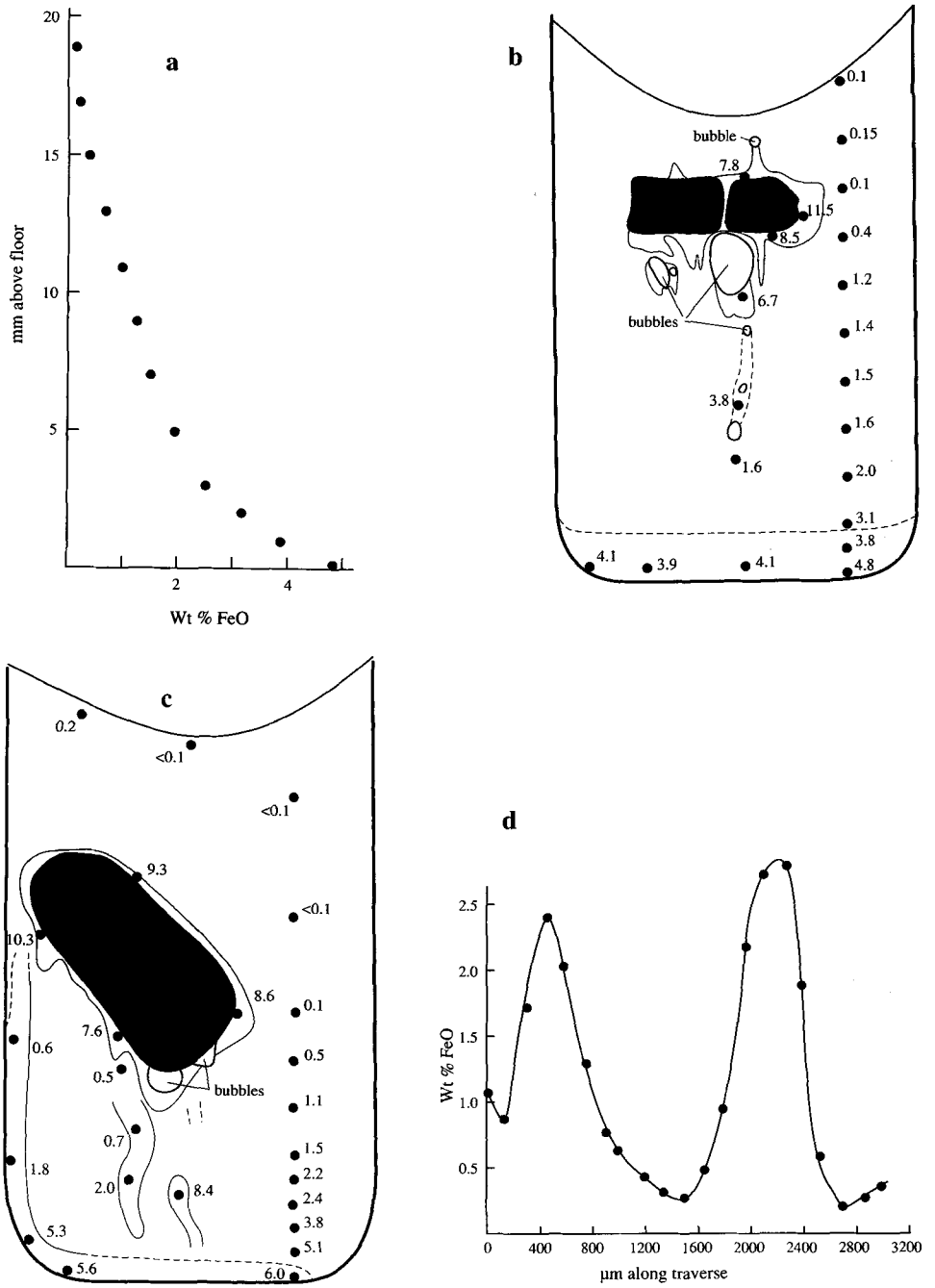

FIG. 3. (*a*) Vertical variation in Fe content of glass through charge in Fig. 2*a*. The profile was obtained to the right of centre of the charge. (*b*) Sketch of run product in Fig. 2*d* with spot analyses of iron (as FeO wt.%) indicated. The lines enclose areas where deep-brown glass exists; where the line is discontinuous, the limit of the brown glass is indistinct. Lightly coloured, yellow glass is not illustrated. (*c*) Same for run in Fig. 2*e*. (*d*) Iron content across two columns of brown glass in the run in Fig. 2*b*. The profile was made 7 mm above the base and began to the left of the thicker column.

Table 4: Composition (wt.%) of glass within 10μm of crystal (first column) and most Fe-rich glass at the base of the same crucible (second column).

	CMAS-mgt 1450°, 0.5hr		CMAS-hmt 1450°, 0.5hr		CAS-mgt 1330°, 2hr		Basalt-mgt 1325°, 8hr	
SiO_2	35.1	37.0	32.6	34.6	46.7	51.6	46.2	49.1
TiO_2	0.3	0.2	0.3	0.3	0.5	0.3	1.9	1.7
Al_2O_3	13.5	14.8	11.3	12.8	11.2	12.0	14.0	15.7
FeO	11.5	6.6	13.4	8.3	21.5	12.0	15.6	12.9
MgO	13.9	14.0	14.3	14.6	0.4	0.2	6.3	5.7
CaO	25.7	28.2	27.7	28.9	18.8	22.5	10.7	9.2
Na_2O[a]	-	-	-	-	-	-	2.4	2.9
K_2O[a]	-	-	-	-	-	-	0.8	1.0
Total	100.00	100.8	99.6	99.5	99.1	98.6	97.9	98.2

a < 0.1 wt.% in CMAS and CAS glasses

Large bubbles have not been seen adhering to the upper surface of a crystal.

CAS system

Most of these run products are also differentiated, with dark brown, Fe-enriched glass lying on the base of the crucible. Charges in which a crystal has not wholly dissolved may contain columns of brown glass which indicate that contaminated melt from immediately around the crystal flowed down to the floor (Fig. 4*a,b*). Brown glass adjacent to a crystal has an FeO content up to 20 wt.%, making it, when molten, as much as 8.5% denser than the Fe-free melt (Tables 4 and 5).

The layer of brown glass on the floor of the crucible in Fig. 4*a* has an elongate pillow shape that is deformed on the right by impact of a brown plume with a flattened head. The photograph does not reveal that the layer and the head of the plume are separated by a >0.25 mm-thick layer of colourless glass that has prevented blending of plume and layer. Several lobes of brown glass hang from the underside of the partially dissolved crystal, and that on the right was possibly descending as a plume prior to quenching. These features, together with the evidence that the brown layer on the floor is made of discrete pillows, imply that instabilities in the film of contaminated melt around a crystal grow into plumes that release some melt from the film and then terminate.

Whereas change in glass colour in the CMAS system run products is gradual, in the CAS system changes are comparatively abrupt; the brown layer on the floor of the crucible is sharply bounded, as are the columns of brown glass and the lobes that hang from crystals. This is emphasised by electron probe analyses (Fig. 5*a*). Across a column, analyses reveal zoning, with the most Fe-rich glass in the axis of the column (Fig. 5*b*). There is some indication of reduction in the amount of Fe towards the margin of the layer and upwards through a layer (Fig. 5*a*).

Fig. 4*b* illustrates the arrested dissolution of an inclined crystal. Again there is a brown, Fe-rich layer at the floor of the crucible and at least three columns of brown glass extend down to this layer. One column remains attached to the brown film on the underside of the crystal from which a small lobe hangs down prior to forming a column (Fig. 5*c*). Again, the indications are that columns draining a film have a transient existence.

Bubbles are abundant on top of the charges in Fig. 4*a* and *b*. Most are part of a touching aggregate, i.e. a froth. The photographs do not show that the glass between the bubbles in the froth can be either colourless or delicate brown in colour; the FeO contents of these are *ca.* 0 and 3–5 wt.%, respectively. As in the CMAS system, the otherwise colourless glass above a crystal may contain small blobs of yellow glass (~1 mm

Table 5: Differences in computed density and viscosity between bulk melt and that within 10 μm of the dissolving crystal

	ρ, g cm^{-3}		% change	η, poise		% change	Temperature, °C
	bulk	boundary		bulk	boundary		
CMAS - mgt	2.735	2.828	+ 3.4	3.0	0.8	-73	1430
CMAS - hmt	2.733	2.800	+ 2.5	3.1	1.3	-58	1430
CAS - mgt	2.520	2.732	+ 8.4	6600	60	-99	1330
CAS -hmt	2.525	2.711	+ 7.3	7800	115	-98.5	1300
Basalt-hmt	2.586	2.625	+ 1.5	160	52	-67	1340

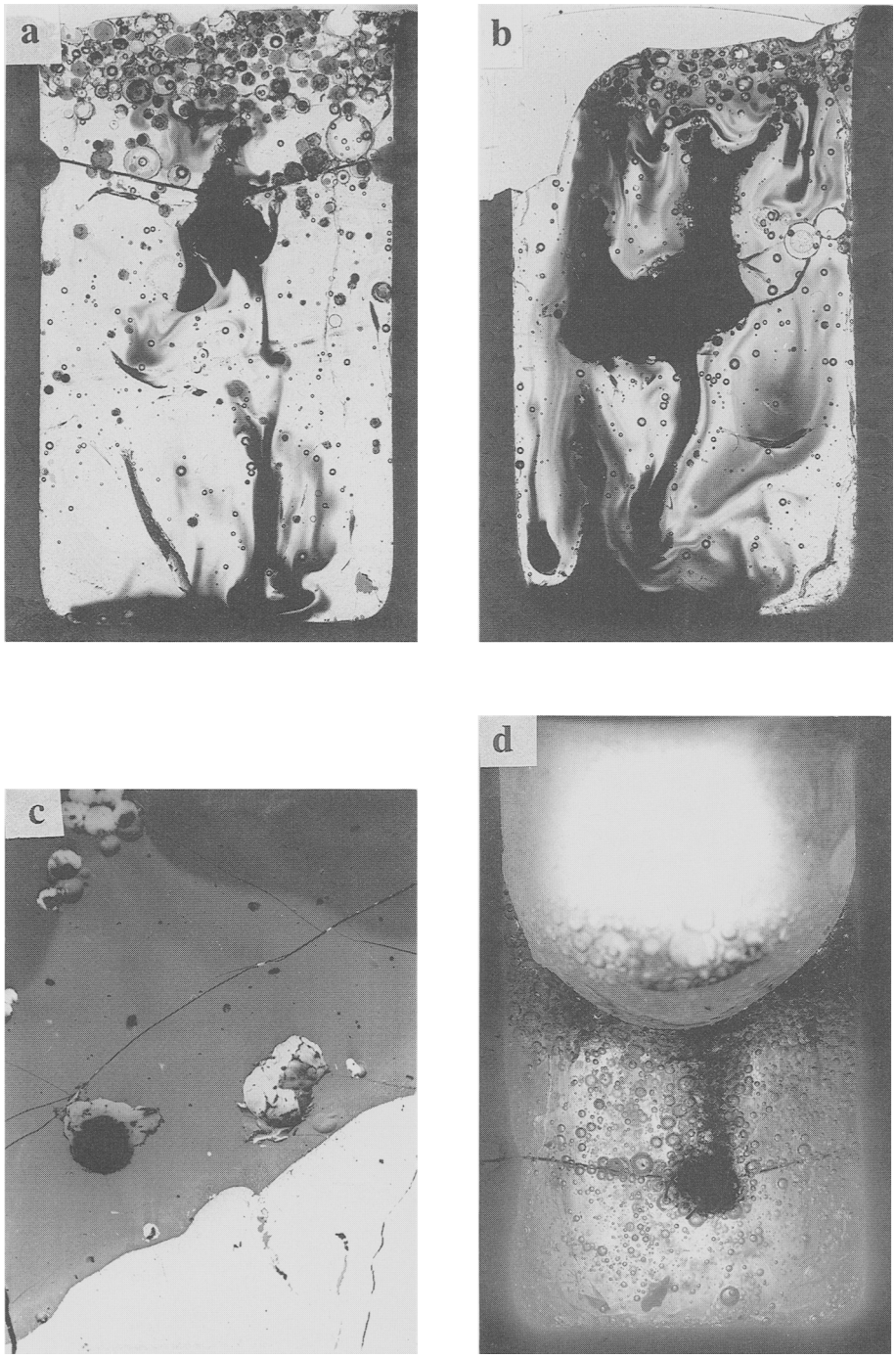

FIG. 4. Selected run products of CAS experiments: (*a*) magnetite, 1330°, 2 hr; (*b*) magnetite, 1330°, 2.0 hr; (*c*) back-scattered electron image of glass adjacent to the top of the crystal in Fig. 4*b*—note the bubbles at the top of the image which have apparently dragged the more Fe-rich (lighter grey) melt in the film upwards (width of view 1.5 mm); (*d*) hematite, 1300°, 2.2 hr.

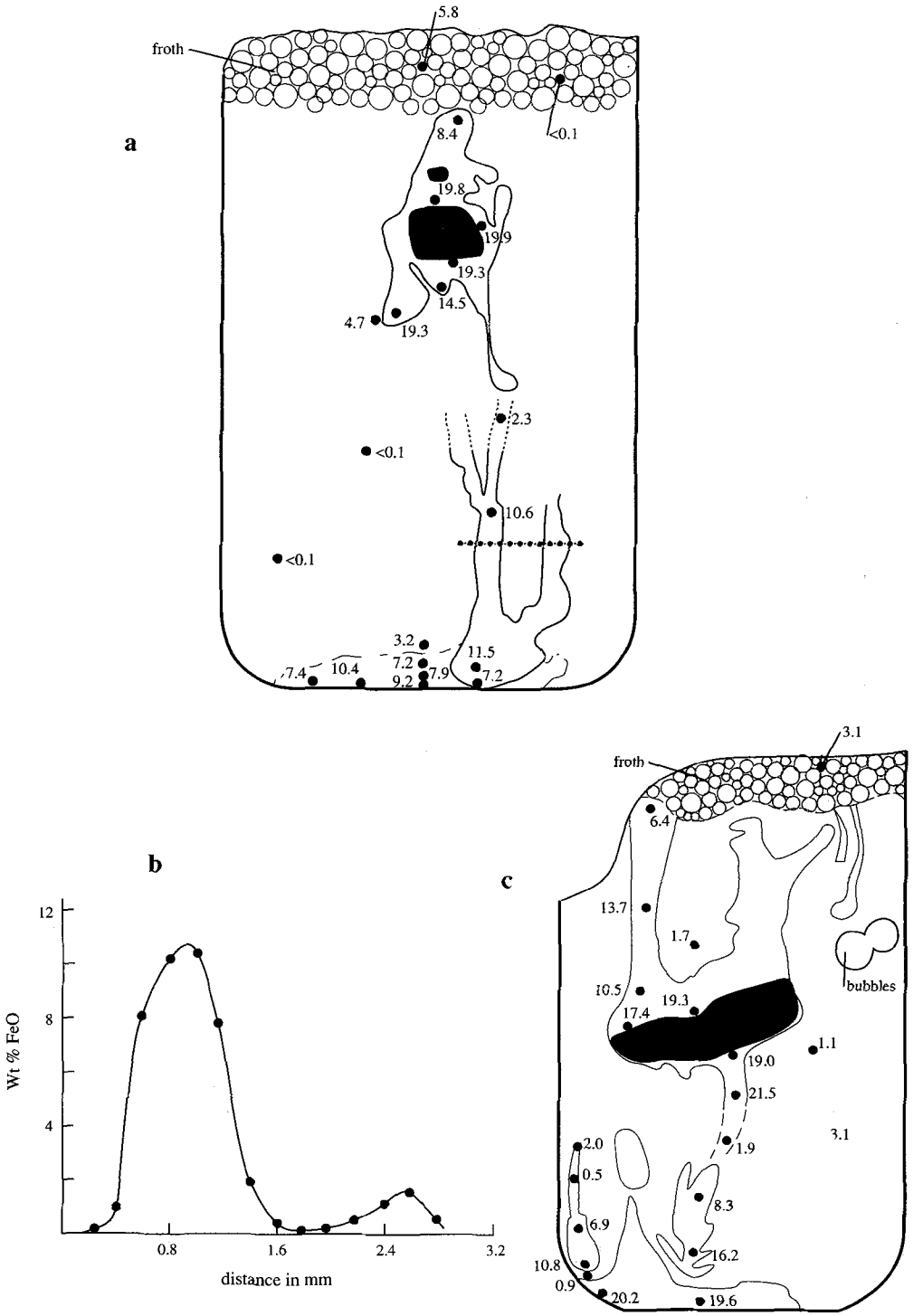

FIG. 5. (*a*) FeO variation in crucible in Fig. 4*a*. (*b*) Traverse across two columns of brown glass (dotted line in Fig. 5*a*). (*c*) FeO content of glass in crucible in Fig. 4*b*.

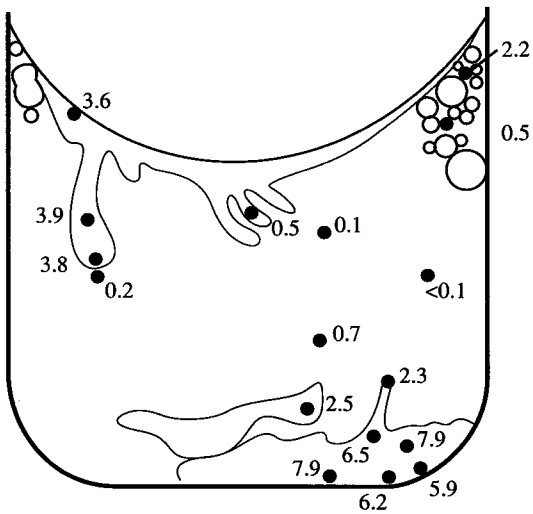

FIG. 6. Sketch of a CAS run with hematite (1300°, 4 hr) in which the crystal has been entirely consumed. A 0.5–1 mm-thick film of brown, Fe-rich glass on the meniscus has several pendulous instabilities; previous instabilities are believed to have settled to the floor to form the pillows there. Spot analyses are FeO wt.%.

across), generally attached to one or more bubbles. Clearly, rising bubbles drag small amounts of the dense, Fe-rich melt from the film around a crystal up into the froth, through which it can spread by Marangoni convection (Considine, 1989), if the Fe-bearing melt has a lower surface tension than the Fe-free melt.

Upward-extending columns containing abundant bubbles have directed the dense melt into the froth (Figs. 4*b*,*c*). The same is true of the run product in Fig. 4*d* in which brown melt has moved from around the crystal into the froth and none has flowed downwards. Fig. 6 illustrates a run product in which a layer of brown glass at the top of the crucible has several lobes hanging down into the colourless glass; evidently the unstable disposition of brown and colourless glasses was being corrected by convective overturn involving descending plumes. By analogy with Fig. 4*d*, the brown layer would have formed by bubbles lifting Fe-rich melt from the film around the crystal into a froth to form an interstitial melt that was almost entirely Fe-bearing; as the bubbles collapsed, so the brown melt became unstable, releasing plumes into the underlying melt which collected as pillows on the crucible floor to build a discrete layer.

Basalt system

Thin sections that do not intersect a crystal have a uniform chestnut-brown colour, identical to that of basalt glass that has not been involved in a dissolution experiment. However, probe analyses reveal slight Fe-zoning (e.g. Fig. 7*a*) with the densest, most Fe-rich glass at the bottom, indicating that melt formed around a crystal has, in each run, migrated preferentially to the bottom of the crucible. Above the level of a crystal, an individual spot analysis may have atypically high Fe-content; these are probably blobs from the Fe-enriched film to a dissolving crystal, floated upwards by bubbles. Bubbles are scarce, and there is never any froth on the meniscus.

In only one run product (B-Mt1) is an accumulation of Fe-enriched melt visible (Figs. 7*b* and 8); a blackish-brown pillow lies on the floor of the crucible, presumably fed from the 400 μm-thick, dark brown film that surrounds the overlying crystal and which has a tail-shaped extension hanging from the underside of the crystal. The pillow is not obviously chemically zoned and has a maximum Fe-content less than that in the film around the crystal. This indicates either that melt from the film mixed intimately with basalt as it flowed to the floor, or that only the outer parts of the film drained away.

This charge shows an additional feature of all the basalt experiments. In contact with the crucible, the glass is yellow rather than brown and is enriched in alumina relative to the basalt, e.g. within 20 μm of the crucible $Al_2O_3 > 23.5$ wt.% versus 15.5% in the basalt. This constitutes another chemical boundary layer, formed by dissolution of the crucible in the basalt. The rate of dissolution must be extremely slow as there is no detectable thinning of the crucible wall, nor any sign of flux-line attack at the crucible-melt contact. The Fe and Mg contents of the yellow glass are less than would be predicted for dissolution of the amount of alumina found, and this is the result of crystallisation of a rind of spinel crystals (78–88 mol.% $MgAl_2O_4$ and 22–12 mol.% $MgFe_2O_4$) on the crucible wall.

The thickness of the yellow boundary layer is more or less uniform along the walls, with the notable exception of the top right of the charge, where it expands into a horizontal, elongate protruberance (Fig. 7*b*). As the density of melt with the composition of the yellow glass within 50 μm of the wall is at least 0.7% less than the basalt, there ought to have been ascent of melt in this boundary layer along the walls, and the protruberance may be attributed to this compositional convection. If correct, it is unclear why the aluminous melt did not reach the meniscus; possibly a difference in surface tension between it and the basalt is responsible.

On the crucible floor the yellow layer is variable

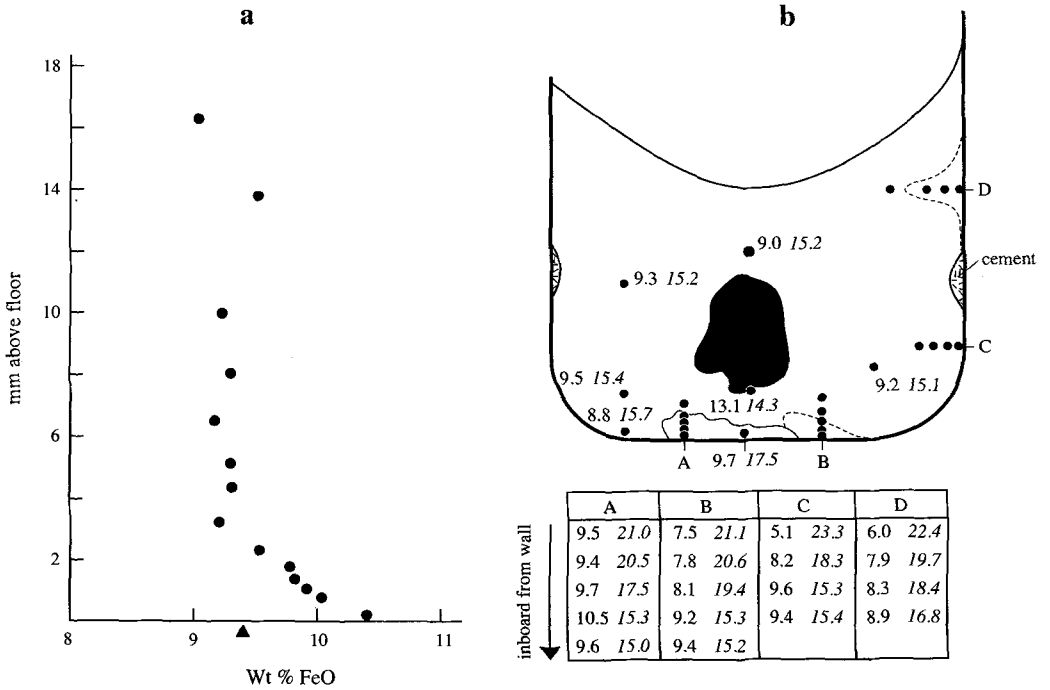

FIG. 7. (*a*) Vertical variation in the Fe content of glass in a run with basalt and a magnetite crystal (1280°, 166 hr). Triangle represents the iron content of the starting basalt. (*b*) Composition variation in run of basalt with magnetite crystal (1315°, 4.5 hr; Fig. 8). The first number in each pair is the FeO content and the second, in italics, is the Al_2O_3 content in wt.%. The area on the floor enclosed by a continuous line is blackish-brown glass. A thin film of yellow glass (~1 mm) separates the crucible from the basalt, with the exception of the two areas outlined by the dashed lines where the thickness of the yellow glass is sufficient to illustrate.

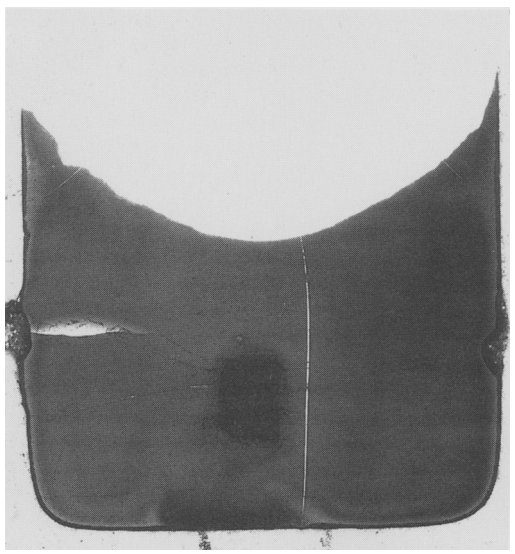

FIG. 8. Crucible containing basalt and magnetite crystal (1315°, 4.5 hr; see Fig.7*a*). Variations in grey reflect colour variations ranging from deep chestnut-brown to yellow.

in thickness (400–900 μm) and has a lumpy upper surface, indicating that incipient plumes exist; however the section shows no lump in the act of escaping the layer, nor is there any discolouration in the overlying glass to suggest that there has been escape of melt.

Discussion and petrological relevance

Contrasts in the zoning of run products

The tactic employed in this study of using Fe-bearing coloured melt to track flow has proved a success. All run products have an asymmetric distribution of Fe and sometimes of colour, consistent with descent of solute-enriched melt from around dissolving crystals. Certain products preserve blobs, streaks and columns of coloured glass that reveal unequivocally the nature of the flow that occurred.

The principal finding of the experiments is that a silicate melt of one composition and density can flow through another and accumulate as a more or less discrete layer, i.e. differentiation by convec-

tive fractionation is demonstrated. The mechanism is revealed to involve columns of melt developing from instabilities in the chemical boundary layer around a dissolving crystal. Since the Fe content of glass in a column always declines to the outside, it is inferred that melt drains from around a crystal in a systematic fashion: melt originally nearest the crystal will occupy the core of a column, whereas the margin will consist of melt originally at the limit of the film of Fe-rich melt surrounding a crystal. This interpretation is supported by the BSE image of the junction between a column and a film (Fig. 9*a*). A column can be considered as the translation of the vertical chemical gradient in a film on the underside of a crystal into a horizontal gradient in the column that drains the film.

The melt that accumulates on the base of the crucible may form a discrete volume in the other. Alternatively, the run product may consist of a single layer that is vertically zoned. Which of these is the outcome in a particular system depends on the contrast in viscosity between the host melt and that in the film generated by crystal dissolution. When host melt and that in the film both have low viscosity, the entire run product is vertically chemically zoned, as exemplified by the CMAS system and perhaps the basalt (Fig. 7*a*). On the other hand, in the CAS system the two melts have a substantial viscosity difference (Table 5) and glasses are sharply chemically separated rather than graded (cf. Kouchi and Sunagawa, 1985).

These differences are ascribed to differing ability of the contrasted melts to blend. One possible situation for blending is during flow of melt within a column. Where a column of coloured glass is preserved in run products, it is always coherent and lacks perturbations. Flow is therefore laminar and steady, which is consistent with the very low values ($<10^{-3}$) for the 'internal' and 'external' Reynolds numbers for plumes in the CMAS- and CAS-magnetite/hematite runs (estimated from equations 1*a* and 1*b* in Huppert *et al.*, 1986). Any mixing would therefore involve shearing at the junction between the column and the Fe-free host melt, with entrainment of the latter in the column resulting in downward thickening of the column. However, columns do not thicken, indicating that there has been no significant entrainment. Entrainment would require Fe from the column to diffuse into the surrounding melt and cause the density of that melt to rise relative to that beyond (cf. Duncan and Richards, 1991). Thus, the absence of entrainment in the experiments is probably due to the slow rate at which chemical diffusion occurs in silicate melts.

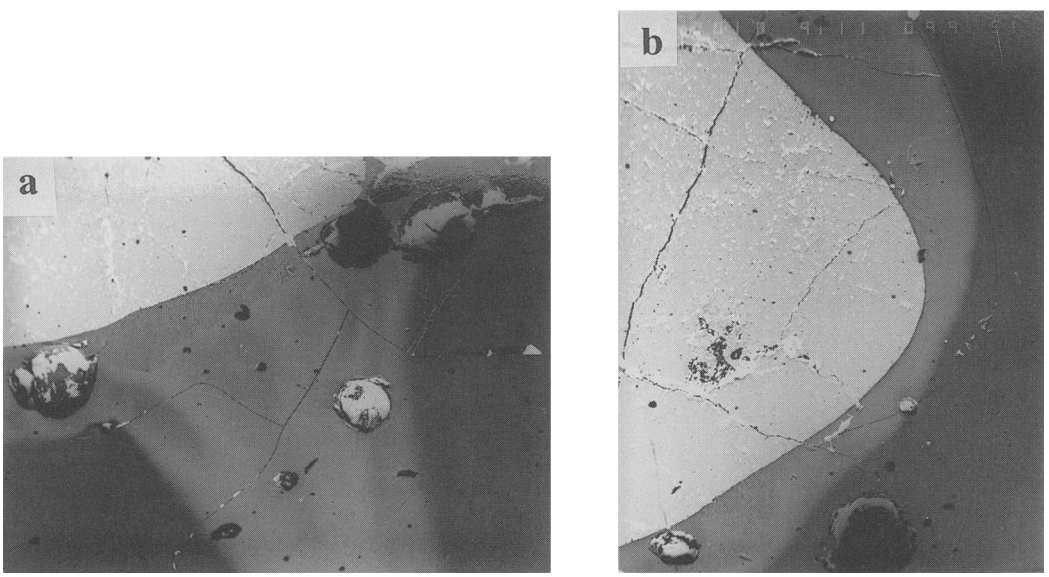

FIG. 9. (*a*) BSE image of the contact between the base of a partially dissolved crystal, the film of surrounding Fe-enriched melt and the column that drains the film (see Figs. 4*c* and 5*c*). Note the bubbles in the film to left and right of the column. Delicate dendrites of magnetite have locally overgrown the crystal on quenching. [Width of view 2.0 mm.] (*b*) Variation in thickness of film of melt at the right-hand coign to the crystal in Fig. 4*b*. [Width of view 1.5 mm.]

Another mixing process can be expected to operate at the base of a column of Fe-enriched melt. Where a column strikes the crucible floor it must be directed outwards; there will be a swirling of melts and some incorporation of each in the other. When the host melt is stiff, swirling will be inhibited, and mixing ineffective.

A quite different process operating at the base of the column, the 'filling-box' mechanism (Baines and Turner, 1972; Leitch, 1990) might account for vertical grading. This has been advanced previously to account for the development of chemical (or temperature) zoning of fluid in a container traversed by plumes. Consider a plume of melt of one composition and density descending through another. Because melt in the axis of the plume is the densest, it descends most rapidly and spreads over the floor. Melt beyond the axis, being less dense, will descend more slowly, and on reaching the layer of denser melt on the floor will delaminate and spread out over that melt. Melt even further beyond the axis will delaminate at even higher level, etc. Thus the unstable density distribution of melt, in the film, on the underside of a dissolving crystal, is turned upside down after melt flows to the bottom of the crucible.

In the CAS system, the absence of vertical chemical zoning in the bulk of the glass in each charge suggests that mixing by swirling either did not occur, because of the high viscosity of the CAS melt, or because it was of feeble strength. On the other hand, the slight zoning in the pillows that exist on the bottom of the charges is consistent with their emplacement by the filling-box mechanism. By contrast, in the CMAS system, brown columns extend down into the brown layer with no obvious thinning of the column (e.g. Fig. 2), i.e. the column is denser than the brown layer; this indicates that mixing by swirling at the impact site of a column is effective in the CMAS system in causing mixing of host melt and column melt. The host melt available for mixing with column melt at the bottom of the crucible will become progressively more Fe-rich and denser, so that the mixed melt will always be denser than its predecessors and lie at the bottom of the charge, having displaced its predecessors upwards. It is stressed that the inferred mixing by swirling in the CMAS system, and probably also in the basalt, must be very effective, for streakiness is not visible in glass at the bottom of crucibles either in optical or BSE images, nor do spot analyses disclose any streaky heterogeneity.

These observations and interpretations mean that blobs or columns of melt (+crystals) descending by laminar flow through a magma chamber to the floor (cf. Morse, 1986) will entrain host melt only slowly. At the floor, this melt will collect and accrete as discrete pillows if there is a substantial viscosity contrast, or will mix with host melt due to turbulent outflow of melt from the base of the column when there is little viscosity contrast. In the latter case, whether or not a vertically zoned layer of melt forms above the chamber floor will depend on how rapidly crystallisation at the floor uses up the new melt relative to the rate at which it arrives there. It is conceivable that this mechanism could trigger abrupt changes in the identity of cumulus minerals forming on the floor of a layered intrusion. For example, small-scale alternations (<30 cm) between olivine- and feldspar-dominated layers in the Rhum intrusion (e.g. Young *et al.*, 1988) might be caused by this mechanism. Because of the orientation of the temperature gradient in the charges, no light is shed, by the experiments, on the possibility of double-diffusive convection and multiple layering of magma in intrusions. Multiple layering is not expected in the experiments and none is visible or detectable by probe analysis.

Manner of release of melt from a film

Bubbles in the film on the underside of a crystal must have been trapped there during ascent through the charge, or have formed *in situ*, either during initial melting of the charge, or subsequently when oxygen produced by hematite-decomposition, or air contained in cracks in the crystal, was released at the crystal–melt interface. These bubbles may help to 'pin' the boundary to a crystal and to inhibit the formation of the lobe-shaped instabilities that develop into plumes. On the other hand, their location probably also determines where instabilities form, e.g. the plume in Fig. 9*a* may have formed preferentially between the bubbles that lie on either side of it. Bubbles might be carried from the film around a crystal down a column to the floor, and some brown glass columns do contain bubbles consistent with this suggestion; however, surface tension between bubble and crystal probably enables most bubbles to remain attached to the crystal.

The film around a crystal is not uniform in thickness, as clearly demonstrated in Fig. 3*b* and *c*. Dissolution should proceed most rapidly where the film is thinnest and most slowly where it is thickest, which, if nothing else happened, would self-correct by adjusting to a condition of uniform film thickness. As this does not happen, melt must move within the film and accumulate on the underside of a crystal. This may seem unreason-

able, for intuitively, one might expect melt at an overhanging coign to fall away from the crystal. However, the absence of a plume from the lower right coign of the crystal in Fig. 5*c* shows that this need not be so. Where a film is thin, it must cling to the sides of crystals, and be prevented from breaking away by viscous forces and adhesion to the crystal.

Whereas CMAS run products containing a relic crystal normally have a brown column extending from crystal to floor, CAS products feature one or more incomplete columns. Thus, flow of melt from the film around a crystal in the CMAS system was apparently continuous, while in the CAS system there was a punctuated release of this melt. This implies that the film was always thick enough to sustain a plume in the CMAS system, whereas in the CAS system the thickness fluctuated with time, growing to a sufficient thickness to release a plume, then falling below the critical thickness causing cessation of the plume, then regrowing until thick enough to permit a new instability to grow into a plume. Thus, the incubation period between cessation of one plume and initiation of another is small or nonexistent for the CMAS system but is significant for the CAS system. This difference is ascribed to faster diffusion of Fe released from a magnetite/hematite crystal through the CMAS melt, as may be expected from the low viscosity of this melt.

Whether there is continuous or punctuated release of melt from around a dissolving or growing crystal will depend on the rate at which the chemical boundary layer is produced, i.e. on dissolution or growth rate. When dissolution, or growth, is slow (i.e. at low undersaturation/supersaturation), punctuated release may be expected; faster dissolution, or growth (at enhanced undersaturation/supersaturation) should encourage continuous draining of the boundary layer. It may further be expected that continuous release will be more likely in mobile, ultrabasic and basic melts, than in stiffer intermediate and acid ones. In the case of crystals that are growing, punctuated release of melt could result in oscillatory zoning in minerals with solid solution (cf. Loomis, 1982).

Each plume is the result of an instability developing in the film around a crystal. The necessary condition for release of melt from a horizontal surface is given by the compositional Rayleigh number, Ra_c, which should exceed a threshold value of *ca.* 2000 (Rosenberger, 1979), where $Ra_c = (g\Delta\rho_c d^3/\mu D)$ g being the gravitational constant, $\Delta\rho_c$ the compositional density difference across the film, d the film thickness, μ the viscosity, and D the chemical diffusion coefficient (Tait and Jaupart, 1990). μ and ρ are computed from the composition of the host melt (cf. Table 2). Measurements of D are not available for the various elements in the melts studied but are likely to be in the range 10^{-5}–10^{-8} cm^2 s^{-1} (Hofmann, 1980), with larger values for the fluid CMAS melt (10^{-5}–10^{-6}), intermediate values for the basalt (10^{-6}–10^{7}), and the lowest values for the CAS melt (10^{-7}–10^{-8}). [Towers and Chipman (1957) report a tracer diffusion coefficient for Si in CAS system melt of 10^{-7} (1450 °C)–10^{-8} cm^2 s^{-1} (1380 °C).]

Table 6 compares the computed values of film thickness, d, with measured values adjacent to the horizontal lower side of a crystal. Taking the d-values for the most likely range of values of the diffusion coefficient for an element, agreement between measured and estimated thicknesses is reasonable, perhaps with a tendency for the actual thickness to be the smaller, which is to be expected as some films were being drained at the time of quenching, while others would have been growing.

When compared to the sizes of crystals frequently produced in experimental studies of crystal-melt systems (often <0.01 cm), the estimated and measured film thicknesses are very much larger. It is little wonder, therefore, that the effects of compositional convection have not previously been noticed by experimentalists, nor are the effects likely to have influenced many experiments.

Table 6 also contains an estimate of the time, τ, needed for growth of a film from zero thickness to the minimum needed for convection (using the relation $\tau \sim d^2/D$). For the most fluid system, CMAS, the times are tens of minutes; for the basalt system it is several hours, and for the CAS

Table 6: Estimated minimum thickness (d) of a boundary layer to a horizontal crystal face needed for convection, as obtained from the Ra_c equation, and comparison with observed values (d_{actual}). τ is the estimated incubation period for growth of a horizontal boundary layer to instability.

	d^a, μm				d^b_{actual}, μm	τ, hr
	D=10^{-5}	10^{-6}	10^{-7}	10^{-8}		
CMAS-mgt	600	290	130	60	500±200	0.1-0.2
CAS-mgt	6270	2900	1350	620	800±300	50-107
Basalt-mgt	3150	1470	680	320	500±200	6-13

[a] Underlined figures span the most likely range of D values

[b] Visual estimates

system more than a hundred hours. These times are totally inconsistent with most of the run durations of <1–<6 hours which nonetheless are sufficient to cause convection. The explanation lies in the fact that the computed values of τ assume that a horizontal boundary layer grows only by diffusional transport. However, as discussed earlier in this section, there is evidence that boundary layer melt adjacent to inclined faces flows round to the lower horizontal face to increase the boundary layer thickness there. Thus the computed τ values are maximum estimates of the time needed for an instability to develop.

The conditions favouring continuous rather than periodic release of melt from a chemical boundary layer may be inferred from the Rayleigh_c equation and that for estimating τ and include: (*a*) low viscosity of the host melt, making for (i) a small critical value of d because of the low resistance to flow, and (ii) rapid chemical diffusion to rebuild the boundary layer; (*b*) large undersaturation of the host melt with respect to the dissolving solid making for rapid dissolution; and (*c*) a large difference in composition between host melt and boundary layer melt to make the latter as relatively dense as possible for the minimum film thickness. In their description of the development and movement of melt from around growing crystals, Martin *et al.* (1987, Fig. 7*a*) foresaw the continuous streaming of melt but not the punctuated release of packets. For the general case of a crystal growing with no face perfectly horizontal, they depict light melt in the boundary layer moving up along the sub-vertical sides and being released in a plume from the highest coign on the crystal. In contrast, it is not clear in the experiments reported here, that the lowest coign is necessarily that from which heavy melt escapes, even in the continuous streaming situation. Rather, it would appear to be possible anywhere on the lowermost surface, and Fig. 2*e* shows that melt in the film adjacent to an overhanging surface can escape spontaneously by growth of an instability at any position.

Effect of bubbles

In the CAS system, brown glass columns extending from crystal to crucible floor indicate that melt in the boundary layer to a crystal can flow directly to the floor. However, it can also be transported by bubbles to the crucible top from where it is released as the bubbles collapse. This reversing of the flow of dense melt by bubbles might arise in magma chambers that are undergoing a combination of vesiculation and crystallisation. For example, once plagioclase joins olivine as a crystallising phase in mid-ocean ridge basalt, the residual melt becomes more dense (Sparks *et al.*, 1980; Stolper and Walker, 1980); furthermore, Bottinga and Javoy (1990) have emphasised the need for massive degassing of CO_2 from MORB before and during eruption. It is possible that the eruption of dense FeTi basalts from MORB chambers could be assisted by individual bubbles or rafts of bubbles transporting this otherwise dense melt to the top of a chamber, from whence it is erupted.

A magma capable of melting or dissolving wall rocks containing micas and/or amphiboles might also produce a melt containing bubbles which would raft the melt to the chamber roof, even though the melt might be denser than the magma. During degassing, the dense melt would be released in packets and will more or less mix into the host magma, possibly creating chemical zonation.

Petrographic evidence of the influence of bubbles in lifting dense packets of melt and crystals in a solidifying magma has been presented by Helz (1987) and recognised as a factor causing differentiation of the Kilauea Iki lava lake.

In a chamber in which light melt was produced by dissolution or crystallisation, bubbles would speed its movement and help to ensure its survival for accumulation at the roof, relatively unmodified.

Prospects for convective fractionation accompanying crystallisation

Although the experiments conducted have been of dissolution type, they give no reason to doubt that convective fractionation will also be possible during crystallisation, if films around crystals have the necessary buoyancy (or negative buoyancy) to overcome viscous stresses. Indeed, in the experiments with basalt, the growth of spinel on the crucible walls assisted the production of a reduced density boundary layer within which melt ascended and spread out under the meniscus (Fig. 8). Such runs demonstrate that differentiation is possible by sidewall crystallisation, cf. McBirney (1980). The two patches of lighter coloured glass at the base of the crucible in Fig. 8 are incipient plumes which bring to mind the proposition of Helz *et al.* (1989) that packets of low-density, Fe-depleted melt rose within the Kilauea Iki lava lake from the base to the top of the solidifying melt lens.

It should be noted that Martin and Campbell (1988) and Martin *et al.* (1987) have argued that, ordinarily, the film around a crystal growing in a magma will need to be thicker than the size of the

crystal to achieve the necessary buoyancy for convective fractionation. Where crystals are growing slowly on a substrate, as on the floor of an intrusion, a single compositional boundary layer exceeding the thickness of the crystals and blanketing them all will have to form before plumes can escape. Only if crystal growth on the substrate is very rapid, due to extreme supersaturation, are individual crystals likely to release their own plumes.

The issue of particular petrological interest is whether or not crystallisation can release melt substantially different in composition from the host, for accumulation by convective fractionation. For example, Brophy (1990) has appealed to sidewall crystallisation of basalt (and to wall-rock melting) to yield a cap of dacite magma atop the basalt.

Data on the composition of films associated with growing crystals are scant and are the objective of current research in this laboratory. The existing data allow an interim assessment of the hypothesis. Glass in contact with olivine in a pillow basalt is at most 1–2 wt.% enriched in SiO_2 compared to the host (Donaldson, 1975); adjacent to plagioclase, the difference is <0.5 wt.% SiO_2 (Bottinga *et al.*, 1966). Growth of these minerals in a basaltic magma chamber would occur at smaller supersaturation than in the pillows, resulting in even smaller differences in composition between melt in contact with a crystal and that beyond. If convective fractionation of such melt occurred, any resulting cap of this magma would barely differ in composition from that of the underlying basalt, especially as the average composition of the actual segregated melt (the 'cup mixing' composition of Trial and Spera, 1990) would differ even less in composition from the basalt.

Hence, for sidewall crystallisation to be an effecive means of creating a cap of melt substantially different in composition from basalt requires that melt in the boundary layer continues to evolve as it ascends, due to progressive cooling and continuous sidewall crystallisation. Any pluton that evolved in this way should possess in its marginal facies, horizons whose minerals become progressively less refractory when traced upwards. To my knowledge, no pluton has been studied in sufficient detail to test for such cryptic variation within a horizon. However, there is some indication of it in data for the Skaergaard intrusion. Hoover (1989) gives a diagram (his Fig. 10) that compares cryptic variation in the Layered Series (LS) with that in the Marginal Border Series (MBS). This shows, for example, that whereas An_{64} plagioclase is present in the LS at the level of Lower Zone a (at 200 m), there is An_{62} in the LZ a* division of the MBS at the same height, but An_{60} in the same division of the MBS at 3200 m, adjacent to Upper Border Zone α of the Upper Border Series. [For olivine, the respective figures are Fo_{63}, Fo_{59} and Fo_{55}.] Thus, there is an indication that lower temperature minerals were able to crystallise at higher level in the intrusion at the same time as higher temperature ones grew at deeper levels. Nonetheless, the solid solution differences are small and do not suggest that a cap of substantially more evolved melt existed at the top of the lens of magma during solidification of the Lower Zone.

Conclusions

In systems, and under conditions in which a crystal dissolves rapidly in a silicate melt, the experiments support the operation of convective fractionation as a process causing magmatic differentiation (cf. Campbell and Turner, 1987); it is particularly effective in systems in which the product melt of the dissolution is very different to that of the host.

The results show that release of melt can be on either a continuous basis or a punctuated basis. This will be determined by the rate of dissolution and the contrast in viscosity between the product melt and the host melt.

The extent to which the two melts mix, as the product melt moves to the floor of a crucible apparently differs little between systems but there is considerable difference in the extent of mixing as the product melt flows across the floor.

Bubbles are very influential on the progress of an experiment. They can raft dense melt upwards, and in froth they can provide a pathway through which product melt can migrate, if it has a lower surface tension than the host melt. Bubbles may also influence precisely where instabilities may develop in the film of melt surrounding a dissolving crystal.

Despite these demonstrations of the operation of compositional convection in two haplomagmas and a natural magma, the importance of this process as a means of causing differentiation in magma chambers must remain open to question, and needs much more testing against field and petrologic data (cf. Mahood and Cornejo, 1992).

Attempts to demonstrate the operation of compositional convection during laboratory growth of crystals in silicate melt are difficult to conduct. It remains to be seen whether crystals can be grown fast enough to create unstable boundary layers and, if they can, whether it is possible for convective fractionation to occur

when crystals grow at the slow rates to be expected in deep-seated intrusions.

Ackowledgements

I thank David Hamilton for his support, Ed Stephens and Donald Herd for maintaining the electron probe and the journal reviewer for useful comments. The work was supported by NERC grant GR3/6509.

References

Baines, W. D. and Turner, J. S. (1969) Turbulent buoyant convection from a source in a confined region. *J. Fluid Mech.*, **37**, 51–80.

Bottinga, Y. and Javoy, M. (1990) MORB degassing: bubble growth and ascent. *Chem. Geol.*, **81**, 255–70.

—— and Weill, D. (1970) Densities of liquid silicate systems calculated from partial molar volumes of oxide components. *Amer. J. Sci.*, **269**, 169–82.

—— Kudo, A., and Weill, D. (1966) Some observations on oscillatory zoning and crystallization of magmatic plagioclase. *Amer. Mineral.*, **51**, 792–806.

Brearley, M. and Scarfe, C. M. (1986) Dissolution rates of upper mantle minerals in an alkali basalt melt at high pressure: an experimental study and implications for ultramafic xenolith survival. *J. Petrol.*, **27**, 1157–82.

Brophy, J. G. (1990) Andesites from northeastern Kanaga Island, Aleutians. Implications for calc-alkaline fractionation mechanisms and magma chamber development. *Contrib. Mineral. Petrol.*, **104**, 568–81.

Campbell, I. H. and Turner, J. S. (1987) A laboratory investigation of assimilation at the top of a basaltic magma chamber. *J. Geol.*, **95**, 155–72.

Carruthers, J. R. (1976) Origins of convective temperature oscillations in crystal growth melts. *J. Crystal Growth*, **32**, 13–26.

Considine, D. M. (1989) Froth. In *Science Encyclopedia*. Van Nostrand, New York, 1243–4.

Coriell, S. R., Cordes, M. R., Boettinger, W. J., and Sekerka, R. F. (1980) Convective and interfacial instabilities during unidirectional solidification of a binary alloy. *J. Crystal Growth*, **49**, 13–28.

Deer, W. A., Howie, R. A., and Zussmann, J. (1964) *Rock-Forming Minerals*, Vol. 5. Longmans London.

Donaldson, C. H. (1975) Calculated diffusion coefficients and the growth rate of olivine in a basalt magma. *Lithos*, **8**, 163–74.

—— (1985) The rates of dissolution of olivine, plagioclase and quartz in a basalt melt. *Mineral. Mag.*, **49**, 683–93.

—— (1986) Mineral dissolution rates in a superheated basalt melt. *Mat. Sci. Forum*, **7**, 267–74.

—— and Hamilton, D. L. (1987) Compositional convection and layering in a rock melt. *Nature*, **327**, 413–15.

—— and Henderson, C. M. B. (1988) A new interpretation of round embayments in quartz crystals. *Mineral. Mag.*, **52**, 27–34.

Duncan, R. A. and Richards, M. (1991) Hotspots, mantle plumes, flood basalts and true polar wander. *Revs. Geophys.*, **29**, 31–50.

Grout, F. F. (1918) Two-phase convection in igneous magmas. *J. Geol.*, **26**, 481–99.

Helz, R. T. (1987) Differentiation behavior of the Kilauea Iki lava lake, Kilauea volcano, Hawaii: An overview of past and current work. In: *Magmatic Processes: Physicochemical Principles* (Mysen, B. O., ed.). Geochem. Soc. Spec. Publ., **1**, 241–58.

—— Kirschenbaum, H., and Marinenko, J. W. (1989) Diapiric transfer of melt in Kilauea Iki lava lake, Hawaii: a quick, efficient process of igneous differentiation. *Geol. Soc. Amer. Bull.*, **101**, 578–94.

Hofmann, A. W. (1980) Diffusion in natural silicate melts; a critical review. In *Physics of Magmatic Processes* (Hargraves, R. B. ed.). Princeton Univ. Press, pp. 385–417.

Hoover, J. D. (1989) Petrology of the Marginal Border Series of the Skaergaard intrusion. *J. Petrol.*, **30**, 399–440.

Huppert, H. E., Sparks, R. S. J., Whitehead, J. A., and Hallworth, M. A. (1986) Replenishment of magma chambers by light inputs. *J. Geophys. Res.*, **91**, 6113–22.

Jebsen-Marwedl, H. (1956) 'Faden' im Glas eine Folge 'dynactiven' Verhaltens von Schlieren. *Glastechnische Berichte*, **29**, 269–75.

Kerr, R. C. and Lister, J. R. (1991) The effects of shape on crystal settling and on the rheology of magmas. *J. Geol.*, **99**, 457–67.

Kouchi, A. and Sunagawa, I. (1985) A model for mixing basaltic and dacitic magmas as deduced from experimental data. *Contrib. Mineral. Petrol.*, **89**, 17–23.

Kuo, L.-C. and Kirkpatrick, R. J. (1985*a*) Kinetics of crystal dissolution in the system diopside–forsterite–silica. *Amer. J. Sci.*, **285**, 51–91.

—— —— (1985*b*) Dissolution of mafic minerals and its implication for the ascent velocities of peridotite-bearing basaltic magmas. *J. Geol.*, **93**, 691–700.

Lawrence, M. and Birnie, S. (1989) A schlieren system in low-powered microscopy. *Microscopy and Analysis*, 49–54.

Leitch, A. M. (1990) Free convection in laboratory models. *Earth Sci. Revs.*, **29**, 369–83.

Levin, E. M., Robbins, C. R., and McMurdie, H. F. (1969) *Phase diagrams for Ceramists*. Amer. Ceram. Soc., Columbus, Ohio.

Loomis, T. P. (1982) Numerical simulations of crystallization processes of plagioclase in complex melts: the origin of multiple and oscillatory zoning in plagioclase. *Contrib. Mineral. Petrol.*, **81**, 219–29.

Mahood, G. A. and Cornejo, P. C. (1992) Evidence for ascent of differentiated liquids in silicic magma chamber found in granitic pluton. *Trans. Roy. Soc. Edin.*, **83**, 63–70.

Martin, D. and Campbell, I. H. (1988) Laboratory modeling of convection in magma chambers: crystallization against sloping floors. *J. Geophys. Res.*, **93**, 7974–88.

—— Griffiths, R. W., and Campbell, I. H. (1987) Compositional and thermal convection in magma chambers. *Contrib. Mineral. Petrol.*, **96**, 465–75.

McBirney, A. R. (1980) Mixing and unmixing of magmas. *J. Volcanol. Geoth. Res.*, **7**, 357–71.

—— and Noyes, R. M. (1979) Crystallization and layering of the Skaergaard intrusion. *J. Petrol.*, **20**, 487–554.

—— Baker, B. H., and Neilson, R. H. (1985) Liquid fractionation. 1. Basic principles and experimental simulations. *J. Volcan. Geoth. Res.*, **24**, 1–24.

Mo, X., Carmichael, I. S. E., Rivers, M., and Stebbins, J. (1982) The partial molar volume of Fe_2O_3 in multicomponent silicate liquids and the pressure dependence of oxygen fugacity in magmas. *Mineral. Mag.*, **45**, 273–45.

Morse, S. A. (1986) Thermal structure of crystallizing magma with two-phase convection. *Geol. Mag.*, **123**, 205–14.

Rice, A. R. (1981) Convective fractionation: a mechanism to provide cryptic zoning (macrosegregation), layering, crescumulates, banded tuffs and explosive volcanism in igneous processes. *J. Geophys., Res.*, **86**, 405–17.

Rosenberger, F. (1979) *Fundamentals of Crystal Growth 1. Macroscopic Equilibrium and Transport Concepts*. Springer-Verlag, Berlin, 519 pp.

Shaw, H. R. (1972) Viscosities of magmatic silicate liquids: an empirical method of prediction. *Amer. J. Sci.*, **272**, 870–93.

Sparks, R. S. J., Huppert, H.E., and Turner, J. S. (1984) The fluid dynamics of evolving magma chamber. *Phil. Trans. R. Soc. Lond*, **A310**, 511–34.

—— Meyer, P., and Sigurdsson, H. (1980) Density variation amongst mid-ocean ridge basalts: implications for magma mixing and the scarcity of primitive lavas. *Earth Planet. Sci. Letts.*, **46**, 419–30.

Stolper, E. and Walker, D. (1980) Melt density and the average composition of basalt. *Contrib. Mineral. Petrol.*, **74**, 7–12.

Tait, S. R., Huppert, H. E., and Sparks, R. S. J. (1984) The role of compositional convection in the formation of adcumulate rocks. *Lithos*, **17**, 139–46.

—— and Jaupart, C. (1989) Compositional convection in viscous melts. *Nature*, **338**, 571–4.

—— and Jaupart, C. (1990) Physical processes in the evolution of magmas. In: *Reviews of Mineralogy* **24**. *Modern Methods of Igneous Petrology* (Nicholls, J. and Russell, J. K. eds.). Mineral. Soc. Amer. pp. 125–52.

Towers, H. and Chipman, J. (1957) Diffusion of Ca and Si in a lime-alumina slag. *Trans. AIME*, **209**, 769–73.

Trial, A. F. and Spera, F. J. (1990) Mechanisms for the generation of compositional heterogeneities in magma chambers. *Geol. Soc. Amer. Bull.*, **102**, 353–67.

Young, I. M., Greenwood, R. C., and Donaldson, C. H. (1988) Formation of the Eastern Layered Series of the Rhum complex, northwest Scotland. *Can. Mineral.*, **26**, 225–33.

[*Manuscript received 10 June 1992: revised 10 November 1992*]